Bremsstrahlung Differential Cross-Section Measurements for 0.5- and 1.0-Mev Electrons*†

J. W. Motz
National Bureau of Standards, Washington, D. C.
(Received August 19, 1955)

The bremsstrahlung cross section, differential in photon energy and angle, has been determined by measuring the x-rays emitted from thin targets of beryllium, aluminum, and gold, for incident electron energies of 0.5 and 1.0 Mev, with a 5-inch diameter, 4-inch long NaI(Tl) scintillation spectrometer at angles of 0, 10, 20, 30, 60, 90, and 120 degrees. The results show that in this energy region, the Bethe-Heitler-Sauter (Born approximation) theory underestimates the cross section. A comparison of the cross section for beryllium and aluminum gives evidence for electron-electron bremsstrahlung. The experimental values for the Heitler parameter $\phi_{\text{rad}}/\bar{\phi}$ with a gold target are 10 at 1.0 Mev and 9.5 at 0.5 Mev. The low-Z values for $\phi_{\text{rad}}/\bar{\phi}(1+1/Z)$ are 8.8 for beryllium and 8.4 for aluminum at 1.0 Mev and 6.8 for aluminum at 0.5 Mev. The accuracy of these values is estimated to be better than 20%. The corresponding Bethe-Heitler values for $\phi_{\text{rad}}/\bar{\phi}$ are 6.5 at 1.0 Mev and 5.5 at 0.5 Mev.

I. INTRODUCTION

INVESTIGATIONS of the elementary process of bremsstrahlung production have been few and incomplete. On the one hand, the present theory that has been developed to account for the important features of bremsstrahlung radiation depends on the Born approximation except in the extreme energy regions.[1] On the other hand, very few measurements of the bremsstrahlung cross section are available. These measurements mostly involve studies of the energy loss of electrons passing through a material, and in the low-energy region require corrections for the ionization energy loss.

With the development of scintillation spectroscopy, considerable progress has been made in measurements of photon energies and intensities. This technique of photon analysis has been utilized in the present work, which was undertaken to provide detailed experimental information about the bremsstrahlung differential cross section in the low-energy region from 0.5 to 1.0 Mev.

The bremsstrahlung cross section for electrons accelerated in the field of a nucleus has been evaluated by Bethe and Heitler,[2,3] by Sauter,[4] and by Gluckstern and Hull[5] on the basis of the Born approximation. From their results, the cross section at various stages of integration may be designated as

$$d\sigma_{k,\theta}(E_0,k,\theta), \quad [\text{Eq. (11), reference 4; Eq. (4.1), reference 5}]; \tag{1}$$

$$d\sigma_k(E_0,k), \quad [\text{Eq. (16), reference 3}]; \tag{2}$$

$$\phi_{\text{rad}}, \quad [\text{Eq. (28), reference 3}]; \tag{3}$$

where E_0 is the initial total electron energy, k is the photon energy, and θ is the angle between the directions of the incident electron and the emitted photon. Expression (1) is integrated over the direction of the emerging electron and represents the differential form of the cross section with respect to photon energy and angle, without screening. Expression (2) gives the cross section integrated over the direction of photon emission, and expression (3) defines a cross section for the energy lost by radiation, which is given by the quantity

$$\frac{1}{E_0}\int_0^{E_0-\mu} k\left(\frac{d\sigma_k}{dk}\right)dk.$$

In the relativistic region, experimental results have shown better than 10% agreement with the cross section given by expression (2). Such confirmation was obtained for the upper half of the bremsstrahlung spectrum at 60 Mev and 247 Mev by Curtis[6] and Fisher[7] respectively, who used a cloud chamber to measure the energy losses of electrons which passed through thin targets with high atomic number ($Z\approx 80$). In addition, experimental agreement[8] (not in absolute value) with the shape of the photon spectrum predicted by expression (2) has been obtained for electron energies covering a range from about 10 Mev to 300 Mev for both thick and thin high-Z targets.

In the region where the electron kinetic energy is of the order of the electron rest energy, the extent of agreement between existing measurements and the theoretical predictions has not been established. In this energy region the validity of the Born approximation

* Work supported by the U. S. Atomic Energy Commission.
† A preliminary report of this work was given by J. W. Motz and William Miller, Phys. Rev. **96**, 544 (1954).
[1] Theories not depending on this approximation have been given in the nonrelativistic region by A. Sommerfeld, Ann. Physik (5) **11**, 257 (1931), and in the extreme relativistic region by H. A. Bethe and L. C. Maximon, Phys. Rev. **93**, 768 (1954).
[2] H. Bethe and W. Heitler, Proc. Roy. Soc. (London) **146**, 83 (1934).
[3] W. Heitler, *The Quantum Theory of Radiation* (Oxford University Press, London, 1954), third edition, p. 242.
[4] F. Sauter, Ann. Physik (5), **20**, 404 (1934).
[5] R. L. Gluckstern and M. H. Hull, Jr., Phys. Rev. **90**, 1030 (1953).
[6] C. D. Curtis, Phys. Rev. **89**, 123 (1953).
[7] Philip C. Fisher, Phys. Rev. **92**, 420 (1953).
[8] H. W. Koch and R. E. Carter, Phys. Rev. **77**, 165 (1950); J. W. DeWire and L. A. Beach, Phys. Rev. **83**, 476 (1951); Motz, Miller, and Wyckoff, Phys. Rev. **89**, 968 (1953).

becomes more questionable, especially for high Z. Also, it is difficult to accurately evaluate the large effect of electron energy loss and scattering on the intensity and on the angular and energy distribution of the bremsstrahlung radiation in the measurements. Experiments which point up this uncertainty may be summarized as follows:

(a) Measurements[9] were made of electron energy losses due to radiation in cloud chamber gases ($Z=7$, 18, 36, and 54) and in high-Z absorbers[10] with initial electron kinetic energies in the energy region from about 1 to 5 Mev. The experimental values were factors of about 1.5 to 100 larger than theoretical predictions found from expression (3), although it was indicated[11] that at least some of the disagreement could be attributed to the effects of multiple scattering.

(b) In the same energy region, the total energy loss of electrons that were completely stopped in a high-Z thick target was measured with a calorimeter,[12] and the bremsstrahlung intensity produced in such a process was measured with an ionization chamber.[13] The results indicated about 10 percent agreement with theoretical estimates obtained from expression (3). These estimates included corrections for the electron energy loss due to ionization, but did not account for electron backscattering. In addition, different values (33 and 45.5 electron volts) for the energy required to produce an ion pair in air were used in the ionization chamber measurements.[13]

(c) Spectrometer measurements[14] of high-Z thick target bremsstrahlung spectra yielded results that were about a factor of two greater than theoretical estimates which were based on expressions (1) and (2), and which took account of electron backscattering.

The general lack of agreement in the above results indicates the need for more studies in this energy region. It would be particularly desirable to have measurements which do not involve such large corrections for electron multiple scattering before a comparison with the theory can be made.

In the present work, measurements are made of the angular and energy distribution of the bremsstrahlung from low- and high-Z targets for electrons with initial kinetic energies of 0.5 and 1.0 Mev. The bremsstrahlung radiation is measured directly with a scintillation spectrometer, and the targets are thin enough so that the electron scattering and energy loss is negligible. From these measurements, the bremsstrahlung differential cross section with respect to photon energy and angle is determined and compared with the theoretical predictions given by expression (1). A study of the cross section in this differential form constitutes a much more sensitive test of the theory than the integrated forms (2) and (3). Furthermore, this energy range lends itself nicely to such an angular distribution measurement because the radiation intensity is not peaked so sharply in the forward direction, and therefore is not so sensitive to small errors in the photon angle θ. For example, estimates made from expression (1) indicate that for small values of θ, there is only about a 10% difference in the photon intensity for a one-degree error in θ, while at higher energies the difference becomes much larger.

II. EXPERIMENTAL METHOD

A. Apparatus

The experimental arrangement for these measurements is shown schematically in Fig. 1. A beam of monoenergetic electrons is incident on a target of a specific thickness and atomic number Z. The bremsstrahlung emitted from the target at a given angle θ with respect to the incident electron direction, passes to a scintillation spectrometer through a 15-mil aluminum window in the target chamber and a $\frac{3}{8}$-inch diameter, 12-inch long brass collimator.

The electron beam is produced by the National

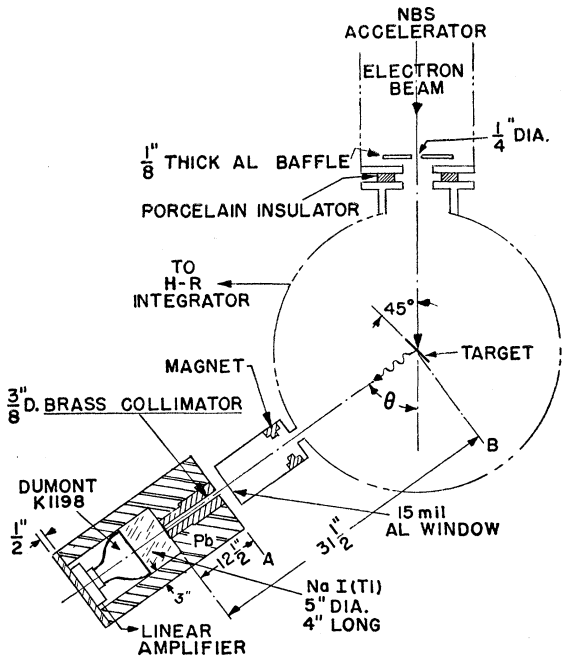

FIG. 1. Experimental arrangement for bremsstrahlung measurements. Initial electron kinetic energies were 0.5 and 1.0 Mev, and values of θ were 0, 10, 20, 30, 60, 90, and 120 degrees.

[9] H. Klarman and W. Bothe, Z. Physik **101**, 489 (1936); L. Leprince-Ringuet, Compt. rend. **201**, 712 (1935); D. Skobeltzyn and E. Stepanowa, Nature **137**, 234 (1936).

[10] J. J. Turin and H. R. Crane, Phys. Rev. **52**, 63 (1937); A. J. Ruhlig and H. R. Crane, Phys. Rev. **53**, 618 (1938).

[11] M. M. Slawsky and H. R. Crane, Phys. Rev. **56**, 1203 (1939).

[12] Ivanov, Walter, Sznelnikov, Taranov, and Abramovich, J. Phys. (U.S.S.R.) **4**, 319 (1941).

[13] Petrauskas, Van Atta, and Myers, Phys. Rev. **63**, 389 (1943); Buechner, Van de Graaff, Burrill, and Sperduto, Phys. Rev. **74**, 1348 (1948).

[14] Miller, Motz, and Cialella, Phys. Rev. **96**, 1344 (1955); K. Liden and N. Starfelt, Phys. Rev. **97**, 419 (1955); N. Starfelt and N. L. Svantesson, Phys. Rev. **97**, 708 (1955).

Bureau of Standards 1.4-Mev cascade-type accelerator.[15] The electron energy is determined from the electrostatic potential of the accelerator, which is measured with a high-resistance voltmeter[15] with an accuracy of approximately one percent. A lens-type magnet coil is used to focus the electrons toward the target position where geometry considerations indicate that the angular spread in the beam is less than 0.5°. In order to align the beam with the center of the target chamber and to prevent any shifting of the beam on the target, it was necessary to introduce a $\frac{1}{8}$-inch thick, $\frac{1}{4}$-inch diameter aluminum defining baffle before the entrance to the chamber. The beam position and size was determined from the visible darkening on exposed glass lantern slides. The slides indicated that the beam diameter at the target position was approximately $\frac{1}{8}$ inch for 1000 kilovolts, and $\frac{1}{4}$ inch for 500 kilovolts.

The target chamber is constructed out of a 14-inch diameter, 10-inch long brass cylinder with $\frac{5}{8}$-inch diameter ports. The ports are spaced at 10° intervals covering a range of θ values from 0° to 130°. Brass plates with 0-rings seal the ports and ends of the cylinder. One end plate contains a bellows-type rotating seal which is used to turn a wheel for the target holders. The targets are mounted on 2-inch diameter thin aluminum frames which are automatically positioned in or out of the beam path at the center of the chamber with the aid of a Yardeny SL-3 Servo-Control unit.

The scintillation spectrometer consists of a 5-inch diameter 4-inch long NaI(Tl) crystal and a Dumont K1198 5-inch diameter photo-multiplier tube. These components were assembled in a steel cylindrical container and mounted inside a brass-lead collimator pot having the dimensions given in Fig. 1. The total weight of the collimator unit is about 1000 lb, and a counterweight is used to swing the collimator pot to any desired angle θ. With radiation incident on the crystal, the integrated pulses from the photomultiplier are fed in succession to a cathode follower, a nonoverloading linear amplifier[16] with an *RC* clipping time of 10 microseconds, and a 12-channel differential pulse-height analyzer. Also at the amplifier output, a scaler is used to count the total number of pulses above a base pulse-height level corresponding to 5 kev. During a run, there is less than a 2% shift in the base line of the analyzer, and less than a 10% maximum variation in the window width of any given channel. For the bremsstrahlung measurements which cover a range of photon energies extending up to 500 kev in one case and 1000 kev in the other, the window widths are set at about 10 kev. The actual window width of each channel is continuously calibrated during a run with a mercury relay type sliding pulser, which is motor driven so that the 60-cps pulse output increases in height at a rate that is constant to better than 1 percent. The over-all resolving time of the system as determined with a double pulse generator, is approximately 10 microseconds. The intensity of the bremsstrahlung radiation is controlled so that the total counting rate from the amplifier for all pulses larger than 5 kev does not exceed 900 counts per second. Therefore, the probability that 2 successive pulses in this energy range will be registered as a single pulse is less than 1%.

[15] E. E. Charlton and H. S. Hubbard, Gen. Elec. Rev. **43**, 272 (1940).

[16] R. L. Chase and W. A. Higinbotham, Rev. Sci. Instr. **23**, 34 (1952).

B. Procedure

With the accelerator operating at 500 and 1000 kilovolts, measurements were made at angles of θ equal to 0, 10, 30, 60, 90, and 120 degrees and 0, 10, 20, 30, and 90 degrees respectively.

The measurements were carried out according to the following procedure. The pulse-height distribution of the scintillation crystal was determined for a particular set of conditions: a given incident electron kinetic energy (500 or 1000 kev), a given target material and thickness, an integrated charge incident on the target, and a given angle θ. For each set of conditions, the pulse-height distribution was measured with the target foil in and out of the electron beam.

For a given incident electron energy E_0, the bremsstrahlung differential cross section with respect to photon energy and angle is determined by the quantity $P(k,\theta)/mn\Omega$, where $P(k,\theta)$ is the number of photons emitted from the target in the solid angle Ω per unit energy interval at energy k and angle θ for n electrons incident on m target atoms per cm^2. The photon flux $P(k,\theta)$ is directly related to the pulse-height distribution measured by the spectrometer. The method of determining each of the above quantities and estimates of the corresponding errors are discussed below.

C. Measurement of Electron Current

Electrons incident on the target are collected by the target chamber as shown in Fig. 1. This chamber is electrically insulated from the grounded section of the accelerator, and serves as a Faraday cup. Only a negligible fraction of the incident electrons can be backscattered out of the chamber because of the small solid angle (less than 0.01 steradian) subtended by the entrance aperture with respect to any point on the chamber wall. Target currents in a range from 10^{-10} to 10^{-6} ampere are measured with approximately 2 percent accuracy with a Higinbotham-Rankowitz type current integrator.[17] The input circuit to the integrator has the property of maintaining the chamber at ground potential. To assure the absence of spurious effects such as the external collection of charge produced by ionization in the air, the chamber potential was varied plus and minus 45 volts with respect to ground, and no change was observed in the target current. The in-

[17] W. A. Higinbotham and S. Rankowitz, Rev. Sci. Instr. **22**, 688 (1951).

tegrator was calibrated with currents in the specified range, which were determined with an accuracy of one percent. The area in the vicinity of the target chamber was surrounded with a ring of lead shielding stands which were grounded to minimize outside electrostatic disturbances. During a run, the target current appeared stable, and frequent checks were made of the zero-target-current setting.

D. Target Materials and Thicknesses

The target materials were selected to test the theory over a wide range of atomic numbers, and included beryllium, aluminum, and gold. The purity of these materials was determined by spectrochemical analysis. Various target impurities were detected in quantities not exceeding a fraction of one percent by weight. Because of the Z^2 dependence of the bremsstrahlung intensity, the relative contribution to the total radiation intensity from these impurities is primarily important for the low-Z targets. This contribution was estimated for the impurities in a given target by the use of the Z^2 impurity-target ratio, and was found to be less than 5% for all of the targets used in these measurements.

A detailed measurement of the bremsstrahlung differential cross section requires thin targets in which the electron energy loss and scattering is negligible. As an aid in the selection of such a thin target the angular spread of the electrons emerging from the target may be compared with the angular spread of the bremsstrahlung radiation. From the results of multiple scattering theory, Blanchard[18] has given a convenient expression for the mean square angle $\bar{\theta}_e^2$ of the electrons emerging from a given target. His results indicate that $\bar{\theta}_e^2 \approx 0.6Z\bar{\Delta}/T_0(T_0+1)$, where the average electron energy loss, $\bar{\Delta}$, is about 2 Mev per g per cm^2 in the present energy range,[19] and T_0 is the initial electron kinetic energy in Mev. For the bremsstrahlung radiation, angular distribution plots obtained with the Sauter theory[4] indicate that the angular spread can be approximated by a Gaussian distribution with a mean square angle $\bar{\theta}_k^2$ of $2/3T_0^2$. From these estimates, a rough guide which can be used in the selection of thin targets, is that $\bar{\theta}_e^2/\bar{\theta}_k^2 \ll 1$, or that the target thickness $t(\text{g/cm}^2) \ll (1/2Z)[(T_0+1)/T_0]$. In order to definitely establish the fact that the targets used in the present study are thin enough, measurements were made with two target thicknesses of gold and of aluminum (see below). The plots of the differential cross section, computed from the measurements for two thicknesses of the same material, agreed within the limits of the experimental error.

The average thickness of each target was determined with one percent accuracy from measurements of the target area and weight. In order to check the uniformity of each target thickness, the target was scanned in $\frac{1}{4}$-inch diameter segments with a polonium α-particle gauge, which measured the relative alpha-particle transmission through the foil. The maximum variation from the average foil thickness was found to be less than 10% over the whole target area and less than 3% over the limited area where the electron beam impinges on the target.

A summary of the targets used in these measurements is given as follows: a 0.22-mg/cm^2 gold foil, a 0.43-mg/cm^2 gold foil, a 0.63-mg/cm^2 aluminum foil, a 1.0-mg/cm^2 aluminum foil, and a 4.3-mg/cm^2 beryllium foil. Because each of these targets was tilted at an angle of 45° with respect to the direction of the incident electron beam (see Fig. 1), it is necessary to use a multiplying factor of 1.4 to obtain the effective target thickness.

E. Geometry Measurements

The important geometrical quantities involved in an absolute determination of the differential cross section are the angle θ (Fig. 1), and the solid angle Ω in which the photons emitted from the target are detected by the spectrometer.

The collimator axis of the spectrometer was set at given values of θ (see Sec. B) with the aid of an index plate. The accuracy of each setting was determined by comparing the angle between the collimator axis and electron beam direction with calibrated angles inscribed on a template. The maximum possible error in a specified θ value was less than 1 degree, and the corresponding error in the photon intensity $P(k,\theta)$ (Part II-B) was about 10%.

The solid angle Ω was determined from the geometry shown in Fig. 1. The area subtended by the spectrometer crystal with respect to the center of the chamber is mainly defined by the $\frac{3}{8}$-inch diameter collimator hole, which gives an angular resolution of about 1°. However, depending on the photon energy, there can be various degrees of photon penetration and scattering through the collimator walls. Such an effect would tend to increase the solid angle. In order to estimate how this effect depends on photon energy, measurements were made with gamma-ray sources, Cs^{137} (0.66 Mev), and Co^{60} (1.17 Mev, 1.33 Mev), placed at position A directly in front of the collimator and at the target position B (see Fig. 1). Because of the difference in solid angle at the two positions, there is a corresponding difference in the relative number of photons which strike the collimator wall. Therefore, if the pulse-height distribution curves measured at the two positions, are normalized to a given source-crystal distance by the use of the inverse square law, the percent change in the effective solid angle in the two cases can be found by the ratio of the curve areas. The results show that the effective solid angle is 14% larger for the Cs^{137} source, and 32% larger for the Co^{60} source, at position A

[18] C. H. Blanchard, in *Electron Physics*, National Bureau of Standards Circular 527 (U. S. Government Printing Office, Washington, D. C., 1954), p. 9.
[19] See reference 3, p. 368.

compared to position B. Additional measurements made with a calibrated Co^{60} source at the target position B (see Sec. G) indicate that the effective solid angle of detection for 1-Mev photons emitted from the target is approximately 10% larger than that computed by using an area equal to the $\frac{3}{8}$-inch diameter hole at the front crystal face. This solid-angle correction was used in the present measurements for 1-Mev photons, and on the basis of the results obtained above with the Cs^{137} and Co^{60} sources, the correction was assumed to have approximately the same dependence on photon energy as the photon penetration that is given by using the total photon absorption coefficient for brass.

F. Determination of the Photon-Flux

The radiation incident on the NaI(Tl) crystal can be separated into two components: (a) the normal background radiation which includes that produced by the electrons incident on the walls of the target chamber, and (b) the photons defined in Sec. B as $P(k,\theta)$, which pass from the target through the $\frac{3}{8}$-inch diameter collimator hole to the crystal as shown by the geometry in Fig. 1. Component (a) is measured with the target foil out of the electron beam, and component (b) is then the difference measured with the foil in and out of the electron beam. In addition to the target itself, other materials in the collimator line of sight can act as potential sources of radiation. These materials include the 15-mil aluminum window of the target chamber and a small region of the opposite chamber wall (Fig. 1). Radiation from the wall region is mainly accounted for by the measurements made with the foil moved out of the electron beam. To eliminate radiation from the window, an electron trap employing a permanent magnet deflects electrons traveling in the direction of the window. The effectiveness of the trap was checked in the following manner: A tantalum foil was placed over the inside area of the aluminum window for values of θ equal to zero degree (where the window is in the direct electron beam) and 20 degrees, and no appreciable difference was detected in the pulse-height distributions for a given target as compared to the cases with no tantalum foil.

The pulse-height distribution produced in the NaI(Tl) crystal by the incident radiation is measured with the differential analyzer, as described in Sec. A. If the pulse heights are calibrated in terms of photon energies, then the pulse height distribution can be expressed in terms of the number of pulses per unit energy interval at a given photon energy. Such a distribution is shown in Fig. 2 for the case where the initial electron kinetic energy is 1 Mev, θ is 30 degrees, the charge of the electrons is 3.5×10^{-6} coulomb, and the target is a 0.43-mg/cm^2 gold foil. The solid line (open circles) represents the pulse height distribution, $N(h)$, produced by the photon flux $P(k,\theta)$. The values for $N(h)$ are obtained from the counting rate difference for the target positioned in and out of the electron beam. The dashed curve shows the target out data which indicates the relative contribution of background radiation over the entire energy range. The effect of the finite spectrometer resolution is shown by the extension of the $N(h)$ curve beyond the maximum photon energy expected for 1-Mev bremsstrahlung.

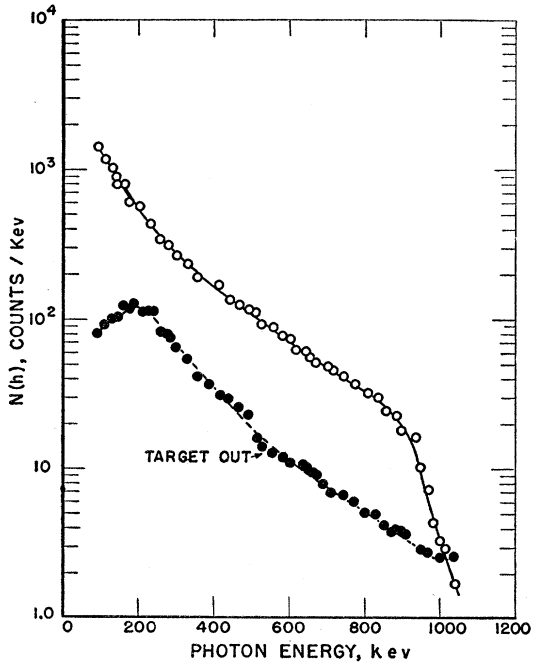

FIG. 2. Pulse-height distribution measured with 1-Mev electrons incident on 0.43-mg/cm^2 gold target for total electron charge of 3.5×10^{-6} coulomb and for θ equal to 30 degrees. The dashed line (closed circles) is the background distribution with the target removed from the electron beam, and the solid line (open circles) is the distribution given by the difference between the target in and out of the electron beam.

For a given photon flux $P(k)$, the pulse-height distribution $N(h)$ can be expressed as

$$N(h)=\int_0^{E_0-\mu} R(h,k)P(k)dk, \tag{4}$$

where μ is the electron rest energy, and $R(h,k)$ is the spectrometer response function which represents the probability that a pulse is recorded in a unit pulse-height interval at height h for a photon of energy k. Approximate solutions of the integral equation for $P(k)$ have been considered for certain analytical response functions.[20,21]

In the present case, the pulse-height response of this large crystal spectrometer to monoenergetic photons has a Gaussian shape with a low-energy tail[22] which

[20] G. E. Owen and H. Primakoff, Phys. Rev. **74**, 1406 (1948); Rev. Sci. Instr. **21**, 447 (1950); J. P. Palmer and L. J. Laslett, Atomic Energy Commission Report AECU-1220, 1951 (unpublished).
[21] Theus, Beach, and Faust, J. Appl. Phys. **26**, 294 (1955).
[22] R. S. Foote and H. W. Koch, Rev. Sci. Instr. **25**, 746 (1954).

replaces the prominent Compton escape peak found with small crystals. Response curves were measured for the photons from sources of Co^{60} (1.17 Mev, 1.33 Mev),[23] Cs^{137} (0.662 Mev),[23] Hg^{203} (0.279 Mev),[23] and Cd^{109} (0.087 Mev).[23] Corrections were made for the background pulse-height distribution which was measured by plugging the collimator hole. The resulting response curves showed good agreement with the theoretical response curves obtained from Monte Carlo calculations by Berger and Doggett.[24] For example, with the gamma rays from thin sources of Cs^{137} and Co^{60} placed at target position B, the response curves gave values of the photo-fraction (defined as the ratio of the photopeak area to the total area under the pulse-height distribution curve) equal to 0.79 and 0.65 (1.33-Mev Co^{60} gamma rays only), compared to the theoretical values of 0.82 and 0.67 respectively. In addition, the measurements indicated that with the source placed at the closer position A (Fig. 1), there was about a 10 percent decrease in the photo-fraction due to the increased scattering in the collimator. The shapes of these curves, which have half-widths that are inversely proportional to $k^{\frac{1}{2}}$ for photon energies below 2 Mev,[22] can be represented as a single universal curve, if the peak values are normalized to one and the abscissas are plotted in terms of the quantity $(h/k-1)\sqrt{k}$. Such a universal shape is plotted in Fig. 3 for the above photon energies. The data shows that the ratio of tail height to peak of the response curve, decreases with photon energy. In the present case, it is a good approximation to assume that the tail height is constant with pulse height for a given photon energy, and a functional relationship can then be obtained between the tail height and photon energy.

With the above information, the response function $R(h,k)$ can be constructed in the form of a matrix with indices h and k, and Eq. (4) can be solved for $P(k)$ by numerical inversion.[20] The matrix elements are determined by adjusting the values obtained from Fig. 3, so that for a given k, $\int_0^\infty R(h,k)dh$ is equal to the detector efficiency. In practise, the matrix elements are summed over h for pulse-height intervals of both 25 and 50 kev. (These intervals were found to be small enough to cause no distortion in the shapes of the computed spectra.) The detector efficiency is given by the quantity $(1-e^{-\mu(k)t})$, where $\mu(k)$ is the total absorption coefficient[25] and t is the length of the NaI(Tl) crystal. If this response matrix is now applied to a given input photon spectrum, a set of simultaneous linear equations is determined which relate the photon spectrum to the corresponding pulse-height distribution.

The accuracy with which values of the photon flux

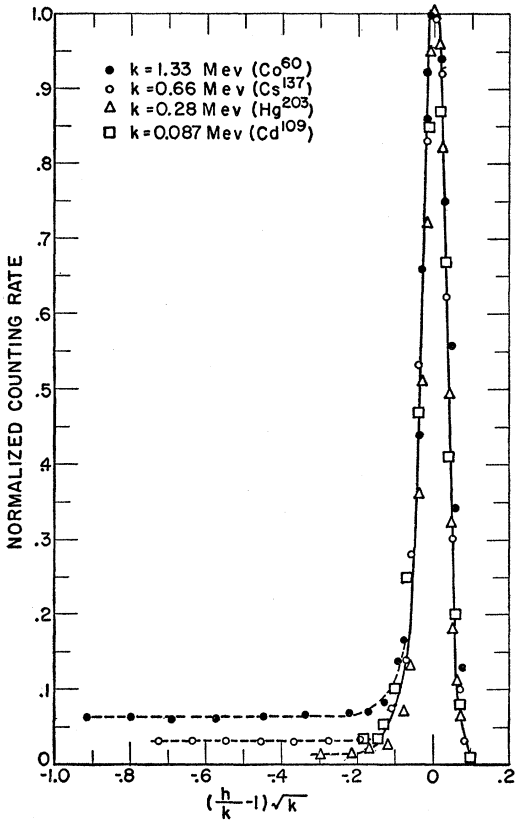

FIG. 3. Universal spectrometer response curves for monoenergetic photons. The measured counting rate is plotted as a function of the pulse height h and the photon energy k. Small fluctuations which appear in the low-energy tail region have been smoothed out to simplify the data analysis.

$P(k)$ can be determined from a measured pulse-height distribution by numerical inversion, depends on the detailed shape of the photon spectrum. In the present case, the measurements indicate that the bremsstrahlung photons have a well-behaved continuous distribution, which falls off rapidly with energy, and which cuts off at a maximum photon energy. The pulse-height distribution data (Fig. 2) have statistical errors that increase up to 30% as the background level is approached in the region of the cut-off point. It is therefore not reliable to carry through the numerical inversion by a simple peeling-off process where the value of the photon flux at a given energy would be critically dependent on the corresponding pulse height value. A more accurate treatment is obtained if it is assumed that the photon spectrum is linear in a small region: then the inversion procedure can be initiated at a pulse-height corresponding to the maximum photon energy, and with the aid of a simple perturbation type calculation, a line by line solution of the simultaneous equations is permissible. Such inversion computations were made for the pulse-height distributions measured with 500- and 1000-kev electrons and with different target materials and photon angles. The resulting correction factor,

[23] *Nuclear Data*, National Bureau of Standards Circular No. 499 (U. S. Government Printing Office, Washington, D. C., 1950).
[24] M. J. Berger and J. Doggett, Rev. Sci. Instr. (to be published).
[25] Gladys R. White, National Bureau of Standards Report NBS-1003, 1952 (unpublished).

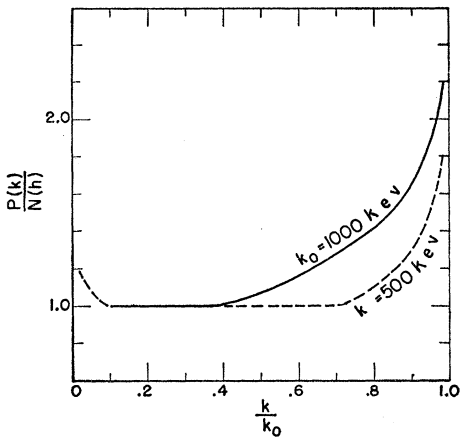

FIG. 4. Spectrometer response correction factor for the bremsstrahlung spectra. Below 100 kev, the correction factor included the effect of absorption by materials (0.24 g/cm² Al and 1.2 g/cm² MgO) in the path of the photon beam before it strikes the NaI crystal.

$P(k)/N(h)$, is plotted in Fig. 4 as a function of the ratio k/k_0, where k_0 is the maximum photon energy. For a given k_0, a single correction curve is obtained for the different cases, probably because all of the spectra have the common property that the flux density $P(k)$ drops sharply with increasing photon energy. Except in the cut-off region of the spectrum, the correction factor is inversely proportional to the photo-fraction (defined above) of the response curve. Because the photo-fraction increases as the photon energy decreases,[24] it is not surprising that the correction factors are smaller for the 500-kev curve. In the region below 100 kev, these curves include a correction which accounts for the photon absorption in the windows of the target chamber and NaI(Tl) crystal, and in the MgO powder that is used as a reflector around the crystal.

G. Calibration Measurements

The photon energies measured by the spectrometer were calibrated with the gamma rays from the radioactive sources listed in Sec. F. Frequent checks on the pulse height stability of the spectrometer were made with the gamma rays from the Co^{60}, Cs^{137}, and Hg^{203} sources, and it was found that the pulse-height corresponding to a given photon energy showed less than a 2 percent variation during a days run. No effects on the energy calibration due to the earth's magnetic field were observed as the spectrometer was rotated into the various positions used in the measurements.

The accuracy with which photon intensities were determined was checked by measurements made with a calibrated Co^{60} source and with cavity ionization chambers. A Co^{60} source was calibrated by the method of gamma-gamma coincidences and the absolute disintegration rate was found to be $(2.03\pm0.01)\times10^7$

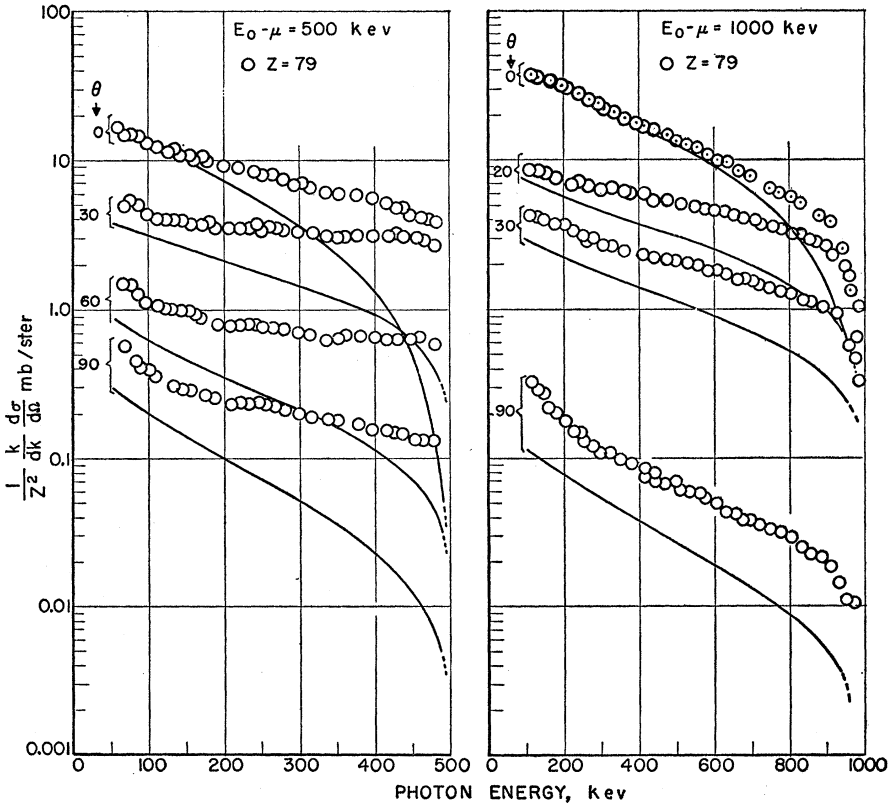

FIG. 5. Differential cross sections for 0.5- and 1.0-Mev bremsstrahlung at photon energies k and angles θ. The experimental values (open circles) were obtained with a gold target. The fractional standard deviations due to statistical counting errors are less than 5% for points below $0.8k_0$, less than 20% for points below $0.9k_0$, and less than 30% for points below k_0, where k_0 is equal to $(E_0-\mu)$. The theoretical cross sections (without screening) are shown by the solid curves which were computed from Sauter's results [see expression (1)].

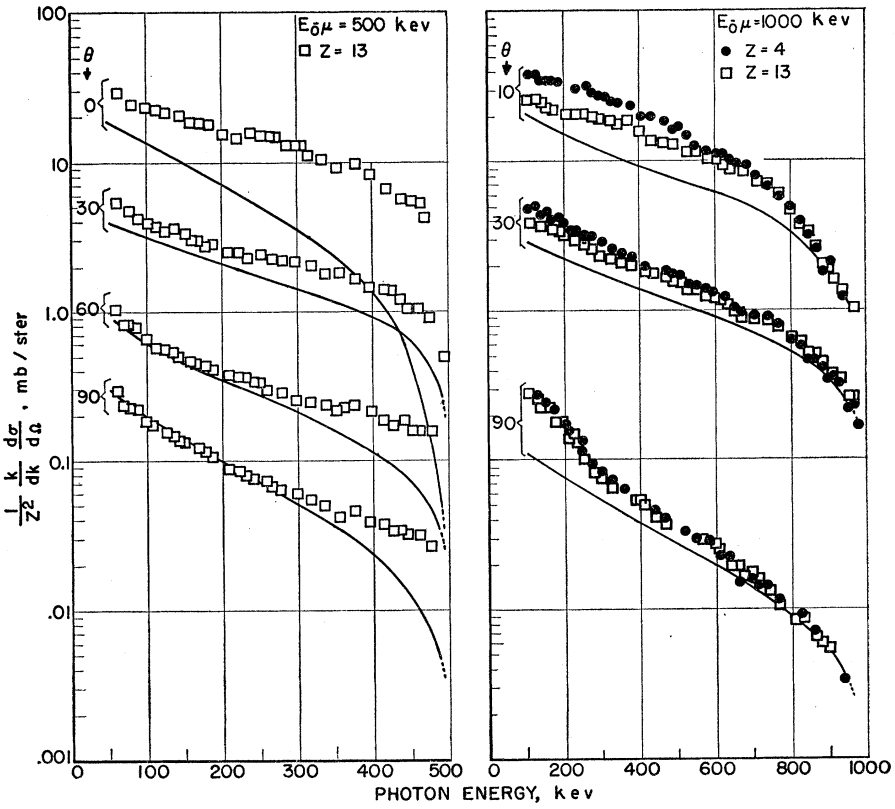

FIG. 6. Differential cross sections for 0.5- and 1.0-Mev bremsstrahlung at photon energies k and angles θ. The experimental values were obtained with beryllium (closed circles) and aluminum (squares) targets, and have the same statistical error limits as discussed in Fig. 5. The Sauter theoretical cross sections (without screening) are shown by the solid curves [see expression (1)].

disintegrations per second.[26] In comparison, the disintegration rate of this source as measured by the spectrometer with the source at the target position was found to be 2.23±0.05 disintegrations per second. This latter result was obtained from the product of the area under the pulse-height distribution curve produced by the Co^{60} gamma-rays, the detection efficiency of the NaI crystal (the absorption coefficient was selected from White's Tables[25] for an average photon energy of 1.25 Mev), and the solid angle correction factor (where the collimator diameter was used to determine the area subtended at the crystal). The 10% excess rate measured by the spectrometer was used as a solid angle correction factor for 1-Mev photons, which arises because of photon penetration through the collimator (see Sec. E).

III. EXPERIMENTAL RESULTS

The experimental values of the differential cross section are divided by Z^2 in order to eliminate the expected Z^2 dependence of the bremsstrahlung radiation. The results are summarized in Figs. 5 and 6, which show the high-Z and low-Z measurements respectively for the initial electron kinetic energies of 0.5 and 1.0 Mev. (Additional results for other values of θ (see Part II-B) are omitted to avoid crowding of the data.) The solid lines in these graphs represent the Sauter theoretical values which are obtained from expression (1) and do not include the effect of screening.

The experimental values of the cross section integrated over the direction of the photon emission are obtained by graphical integration of the results given in Figs. 5 and 6, and are shown in Fig. 7. The theoretical values computed from expression (2) are given by the solid lines.

Finally, the total integrated cross section ϕ_{rad}, which is equal to the quantity $(1/E_0)\int_0^{E_0-\mu} k(d\sigma_k/dk)dk$, was found by integrating the data given in Fig. 7, and is presented in Fig. 8. The theoretical values for ϕ_{rad} are shown by the solid line in Fig. 8, and were obtained from the results given in reference 2. The screening effect which becomes important at the higher energies is shown by the dashed line for $Z=82$. In order to account for the contribution of electron-electron bremsstrahlung, Fig. 8 indicates the shift in the low-Z results that is produced by the factor $Z^2/Z(Z+1)$.

As a final check on the accuracy of the photon flux $P(k,\theta)$ that is determined from the spectrometer measurements, a Landsverk 200-milliroentgen ionization chamber was used to measure the dose produced by the bremsstrahlung radiation at a point on the collimator axis at the front face of the crystal 80 cm from the target. These measurements were made for three different targets, with θ equal to 10 degrees, $(E_0-\mu)$ equal

[26] This calibration was made by Dr. George Minton who is preparing a description of his measurements for publication.

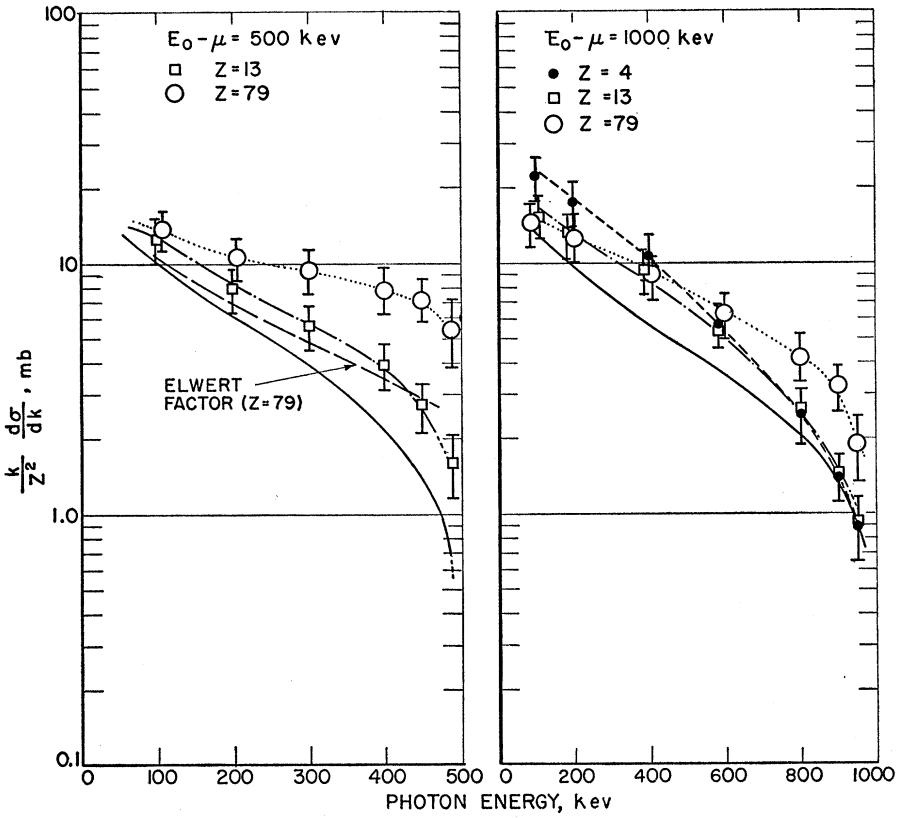

FIG. 7. Cross sections for 0.5- and 1.0-Mev bremsstrahlung integrated over the direction of photon emission. The experimental values were obtained with a gold (open circles), aluminum (squares), and beryllium (closed circles) target, and are shown with the total error limits. The Bethe-Heitler theoretical cross section [see Expression (2)] is shown by the solid lines. The 500-kev Bethe-Heitler curve corrected by the Elwert factor[29] with Z equal to 79 is shown by the dashed curve.

to 1 Mev, and the total electron charge incident on the target equal to 1.7×10^{-3} coulomb. For comparison, the dose was computed from the spectrometer measurements made under the above conditions by integrating the photon energy flux density over photon energy. An approximate conversion factor of 2900 ergs per cm^2 per roentgen was used over this energy range. This value was obtained by using 0.029 cm^2/g for the mass absorption coefficient of air and 33.5 ev for the energy required to produce an ion pair. Also, the dose was computed for the photon energy flux density that would be produced according to the Sauter-Bethe-Heitler theory under the same conditions. The results are shown in Table I, where the accuracy of the values measured by the chamber and spectrometer is estimated to be approximately 10% (see Part IV). The spectrometer measurements show good agreement with the chamber dose measurements compared to the considerably lower values computed from the theoretical cross sections.

TABLE I. Comparison of expected and measured dose 80 cm from target ($E_0-\mu=1000$ kev, $\theta=10°$, $Q=1.7\times10^{-3}$ coulomb).

		Milliroentgens		
Z	Foil mg/cm^2	Landsverk ionization chamber	Spectrometer	Sauter-Bethe-Heitler theory
4	4.3	120	113	60
13	0.63	47	44	30
79	0.43	147	147	110

IV. SUMMARY OF ERRORS

The accuracy of the experimental values obtained for the bremsstrahlung cross sections may be estimated from a survey of the important errors and corrections involved in the measurements.

Sources of systematic error and estimates of the upper error limits are given as follows:

(1) Photon angle (Part II-E): A maximum error of one degree gives a corresponding error of approximately 10% in the value of the photon flux $P(k,\theta)$ (Part II-B).

(2) Target current (Part II-C): $\pm2\%$.

(3) Target uniformity and thickness (Part II-D): $\pm3\%$.

(4) Angle between target plane and incident electron direction (Part II-D): A maximum error of 2 degrees gives a 2% error for the effective target thickness.

(5) Photon flux $P(k,\theta)$ (Part II-F, G): $\pm5\%$.

If these errors were in the same direction, the total error would be $\pm22\%$.

The important corrections made in the measurements include:

(1) Foil impurity correction (Part II-D). The photon intensities $P(k,\theta)$ (Part II-F) measured with the low-Z beryllium and aluminum targets were reduced by 5% to account for the contribution from the high-Z impurities. The reliability of this correction is estimated to be better than 30%.

(2) Solid angle correction (Part II-E). Because of

photon penetration through the collimator, the solid angle computed with the $\frac{3}{8}$-inch diameter collimator was increased by 10 percent for the detection of 1-Mev photons. For decreasing photon energies, the correction decreases in a manner determined by the total photon absorption coefficient for brass. A comparison of the measurements (Part II-E) with the Co^{60} and Cs^{137} sources indicates that this correction is reliable to within 30%.

Other experimental errors are as follows:

(1) Statistical counting errors. The fractional standard deviations for the points given in Figs. 5 and 6 are less than 5% in the energy region below $0.8k_0$, less than 20% between $0.8k_0$ and $0.9k_0$, and less than 30% between $0.9k_0$ and k_0, where k_0 is equal to $E_0-\mu$.

(2) Variation in the window width of the differential analyzer (Part II-A). The fractional standard deviation for the window width is estimated to be less than 4% for any given bin.

(3) Error arising from graphical integration over photon energy and angle of the differential cross section. The maximum uncertainty produced by this integration is estimated to be $\pm 3\%$.

From a consideration of the above errors, it is estimated that the values for the integrated cross section ϕ_{rad} (shown in Fig. 8) are reliable to within 20%.

V. DISCUSSION OF RESULTS

A. Breakdown of the Born Approximation

The theoretical cross sections given in the above results have been formulated on the basis of certain assumptions[27] of which the most important is the Born approximation. The necessary conditions for this approximation are severe: namely that $(2\pi Z/137)(c/v_0)$ and $(2\pi Z/137)(c/v)\ll 1$, where v_0 and v are the electron

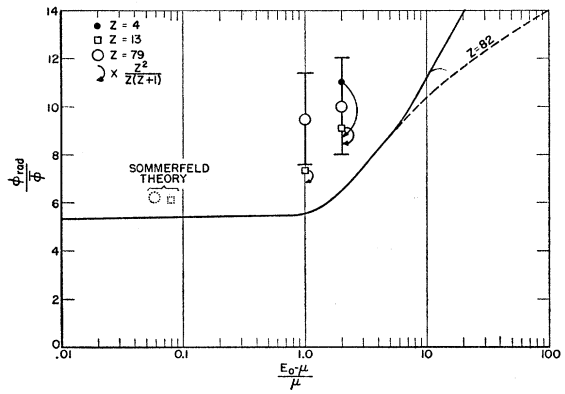

FIG. 8. Cross section for the energy lost by radiation. ϕ_{rad} is equal to $(1/E_0)\int_0^{E_0-\mu} k(d\sigma_k/dk)dk$, where $d\sigma_k$ is given by Expression (2), and $\bar{\phi}$ is $5.8\times 10^{-28}Z^2$ cm^2. The dashed line indicates the screening effect for Z equal to 82. The low-Z experimental values are multiplied by $Z^2/Z(Z+1)$ to account for electron-electron bremsstrahlung. Theoretical values obtained from the Sommerfeld theory[1] are shown in the nonrelativistic region.

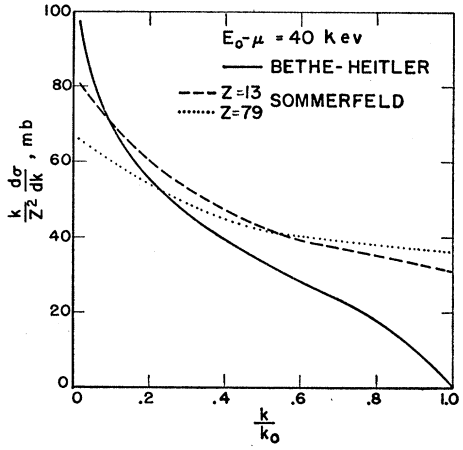

FIG. 9. Comparison of the Bethe-Heitler and Sommerfeld cross sections integrated over the direction of photon emission. The maximum photon energy, k_0, is equal to 40 kev. The Sommerfeld values for the cross section are obtained from the results of Kirkpatrick and Wiedmann.[28]

velocities before and after the collision. Accordingly, the approximation breaks down for large Z.

As v_0 becomes small, the manner in which the differential cross section is modified because of this approximation is difficult to follow intuitively. As a possible aid, it is of interest to compare the exact Sommerfeld theory in the nonrelativistic region with the approximate Bethe-Heitler-Sauter theory.[2–5] Such a comparison provides some grounds for inferring possible qualitative differences between an exact theory and the Bethe-Heitler-Sauter theory at the higher energies $(T_0\approx\mu)$. The Sommerfeld and Bethe-Heitler values of the cross section integrated over the direction of photon emission are plotted in Fig. 9 for an initial electron kinetic energy of 40 kev. The Sommerfeld values for Z equal to 13 and 79 were obtained from the calculations made by Kirkpatrick and Wiedmann[28] and the Bethe-Heitler values were obtained from Eq. (18) in reference 3. A comparison of these curves gives the following information for the nonrelativistic region: (a) The approximate Bethe-Heitler bremsstrahlung theory underestimates the cross section as given by the exact Sommerfeld theory. In the exact theory, the cross section approaches a finite value at the upper limit of photon energies compared to the sharp drop to zero of the Bethe-Heitler curve. At small photon energies, the Bethe-Heitler curve which does not include screening, rises above the exact theory curves. (b) The exact cross sections are not simply proportional to Z^2. At low photon energies, the values of the low-Z curve are greater than the high-Z values, and with increasing photon energies there is a crossover where the low-Z curve drops below the high-Z curve. This crossover feature makes the cross section integrated over photon energies approximately proportional to Z^2. The above

[27] See reference 3, p. 254.

[28] P. Kirkpatrick and L. Wiedmann, Phys. Rev. **67**, 321 (1945).

results provide some clue as to what might be expected in the higher energy region ($T_0 \approx \mu$) where the present measurements were made.

B. High-Z Bremsstrahlung

The high-Z bremsstrahlung results, which are shown in Fig. 5, indicate that the Bethe-Heitler values of the differential cross section underestimate the measured values over most of the range of photon energies. The manner in which the theory departs from the measurements is at least in qualitative agreement with the trend suggested by the results in the nonrelativistic region. The departure of the theoretical curves from the measurements increases consistently as (a) the photon angle of emission θ (or the momentum transfer to the nucleus) increases, (b) the photon energy increases, and (c) the initial electron kinetic energy decreases. The trends (b) and (c) hold also for the cross section integrated over the direction of photon emission, as shown by the results in Fig. 7. The error given for each experimental point in Fig. 7 is an estimated upper limit for the combined errors discussed in Part IV.

Quantitative estimates of the difference expected between the approximate Bethe-Heitler theory and an exact theory were made by Elwert.[29] His results are given as a correction factor that can be applied to the Bethe-Heitler values for the cross section.[30] The Elwert corrected Bethe-Heitler curve is plotted in Fig. 7 for the case where $(E_0-\mu)$ is 500 kev and Z is 79. The large discrepancy that remains between the Elwert curve and the corresponding experimental curve, shows that Elwert's theory does not provide an adequate correction factor for the Bethe-Heitler theory.

Figure 8 shows that the high-Z experimental cross section values for the energy lost by radiation, ϕ_{rad}, are about a factor of two larger than the corresponding Bethe-Heitler values. The high-Z experimental values for $\phi_{\text{rad}}/\bar{\phi}$ (where $\bar{\phi}$ is $5.8\times10^{-28}Z^2$ cm^2) are 9.5 ± 1.9 at 500 kev and 10 ± 2.0 at 1000 kev compared to the theoretical values of 5.5 and 6.5 respectively.

C. Low-Z and Electron-Electron Bremsstrahlung

Low-Z bremsstrahlung is complicated by the fact that the role of atomic electrons becomes important in the process. The cross section dependence is expected to go more like $Z(Z+1)$ rather than Z^2,[31] which means that the contribution from electron-electron bremsstrahlung would be about 10 percent for aluminum and 25 percent for beryllium. The results obtained for these two materials with 1000-kev electrons are shown in Fig. 6. Except for the effect of electron-electron bremsstrahlung, it may be expected that the cross section divided by Z^2 would be approximately the same for all low-Z materials. Therefore, it is difficult to escape the conclusion that the differences shown in Fig. 6 are indeed evidence of the electron-electron bremsstrahlung process. The fact that the differences are large at 10 degrees and practically disappear at 90 degrees carries additional weight, since the radiation intensity from electron-electron bremsstrahlung is expected to be concentrated at small angles from considerations of the dynamics involved in transforming from the center-of-mass to the laboratory system. It is also of interest to determine the maximum photon energy, K_0, for electron-electron bremsstrahlung that is available in the laboratory system at the laboratory angle θ. With the aid of the Lorentz transformation, it can be shown that

$$K_0=\mu F/(1-\cos\theta\sqrt{F}), \tag{5}$$

where F is equal to $(E_0-\mu)/(E_0+\mu)$. From this expression, the values obtained for K_0 with $(E_0-\mu)$ equal to 1000 kev are 824 kev at 10 degrees, 650 kev at 30 degrees, and 253 kev at 90 degrees. These results are not inconsistent with the measurements shown in Fig. 6, where it is seen that the differences between the two materials tend to vanish as the curves approach the above values for K_0.

The low-Z cross section measurements shown in Fig. 6 indicate that even if electron-electron bremsstrahlung is accounted for, there still appears to be some discrepancy between theory and experiment. As θ becomes smaller, the Bethe-Heitler curve underestimates the measured values. For these small values of θ, a comparison of the low- and high-Z curves reveals a cross-over in which the low-Z curve drops from above to below the high-Z curve with increasing photon energies. This behavior which is not revealed in the Born approximation theory is similar to what occurs in the nonrelativistic region for the Sommerfeld theory (see Fig. 9).

The experimental values for the integrated cross section given in Fig. 7 show the combined error for the various factors discussed in Part IV. Most of these cross sections are larger than the theoretical values by an amount that exceeds the error limits. The final low-Z values for ϕ_{rad} are shown without the error limits in Fig. 8. When these values are corrected for electron-electron bremsstrahlung by the factor $Z^2/Z(Z+1)$, they are only about 30% larger than that corresponding theoretical values, compared to the much larger differences obtained in the high-Z results. The experimental values for $\phi_{\text{rad}}/\bar{\phi}$ with the $Z^2/Z(Z+1)$ correction factor are given as 8.8 ± 1.8 and 8.4 ± 1.7 for Be and Al respectively at 1000 kev, and 6.8 ± 1.4 for Al at 500 kev. The corresponding Bethe-Heitler values are 6.5 and 5.5. The Sommerfeld values for ϕ_{rad} are also shown in Fig. 8, and it is seen that like the experimental

[29] G. Elwert, Ann. Physik **34**, 178 (1939).
[30] See reference 3, p. 246.
[31] The $Z(Z+1)$ formula gives only an estimate of order of magnitude. A detailed theory of bremsstrahlung in collisions between free electrons has not been worked out except for limiting conditions, see J. Katzenstein, Phys. Rev. **78**, 161 (1950) and M. L. G. Redhead, Proc. Phys. Soc. (London) **A66**, 196 (1953). For the role of binding in various processes involving atomic electrons, see also J. A. Wheeler and W. E. Lamb, Phys. Rev. **55**, 858 (1939) and U. Fano, Phys. Rev. **93**, 117 (1954).

values at the higher energies, they are larger than the corresponding Bethe-Heitler cross section.

VI. ACKNOWLEDGMENTS

The writer wishes to thank Dr. William Miller for his contributions and suggestions, Dr. H. O. Wyckoff for his help and advice, Mr. Fred Frantz and Mr. George Dempsey for their assistance with the measurements, and Mr. Richard Bach for his help with the calculations. Also, the writer is grateful for the beneficial discussions with Dr. U. Fano, Dr. I. Oppenheim, Dr. M. Danos, and Dr. H. W. Koch.

PHYSICAL REVIEW VOLUME 100, NUMBER 6 DECEMBER 15, 1955

Small Oscillation Theory of the Interaction of a Particle and Scalar Field

E. P. GROSS
Syracuse University, Syracuse, New York
(Received July 28, 1955)

We study the interaction of a nonrelativistic particle with a scalar field, with particular application to the theory of polarons. The approach is based on a general classical method for the integration of equations of motion. The Hamiltonian is transformed by successive canonical transformations, the first corresponding to describing the motion relative to special solutions of the equations of motion. This stage as applied to suitably ordered Heisenberg equations of motion is identical with intermediate coupling theory. The second transformation treats the coupled small oscillations of particle and field oscillators about the chosen special solution. This affords a natural extension of intermediate coupling theory for this problem. Differences between the classical and quantum theories arise in the ordering of operators; the differences play a crucial role in determining the effective cutoff in wave vector space.

1. INTRODUCTION

THE theory of the interaction of an electron with lattice vibrations has received much attention recently. Aside from the question of oversimplifications customarily made in describing the physical system, there is the problem of finding quantum theoretic methods powerful enough to analyze the structure of the typical Hamiltonians encountered. The present deficiency hampers progress in the theory of normal and super conducting metals at low temperatures, and makes uncertain, estimates of lattice mobility in polar crystals and semiconductors. The electron-lattice interaction is also interesting from the point of view of the theory of elementary particles. The Hamiltonian corresponds to a simplified nonrelativistic field theory with a *bona fide* cutoff. One is concerned with developing theories of source recoil for intermediate and strong coupling which may have implications for the general theory of fields. The studies have already given rise to a new adiabatic theory.[1]

We will here be chiefly concerned with the polaron problem—loosely speaking, the theory of the interaction of a free electron with the optical modes of a polar lattice. It possesses the simplification that a minimum energy $\hbar\omega$ is required to excite a quantum of optical vibration (ω is the common frequency of the vibrations). For the lowest states of the system, one has a pure self energy situation with no free quanta present. A range of such states is possible; they are characterized by an integral of the motion $\mathbf{P}$ with the dimensions of a momentum, where $\mathbf{P}$ satisfies $P^2/2m \lesssim \hbar\omega$. Most studies[2–5] have dealt with the properties of the above class of states as a function of coupling strength, in particular the energy of the very lowest state with $P=0$, and the nearby states for which $P^2/2m \ll \hbar\omega$. Less attention has been paid to the case where $P^2/2m \approx \hbar\omega$ and to the nature of the excited states. These regions are of interest in the theory of dielectric breakdown and in mobility calculations. The determination of the energies of the low-lying states has involved mainly variational techniques. The most successful methods are those of Hohler and Feynman. The advantages are known; the disadvantages are that it is hard to make a picture of the behavior, that the intrinsic structure of the Hamiltonian is lost sight of and that the determination of the excited states is made difficult.

In the following, we note that classical theory points to a natural attack on the problem, and we explore some of the consequences. In the theory of orbits one finds a solution of the equations of motion (stable orbit) for which the initial conditions have been chosen in a particular way. Then one studies small oscillations about the orbit. If the orbit is stable, there is a region of phase space in which the full freedom in choice of initial conditions is present. At the edges of the region of stable motion the small-oscillation assumption is not valid; however, classically the amplitude may be made arbitrarily small so that there is always a domain where anharmonic terms can be neglected. For the

[1] N. Bogoliubov, Ukr. Math. J. T II, No. 2, 3 (1950); S. Tyablikov, Zhur. Eksptl. i Teort. Fiz. 21, 377 (1951).

[2] S. I. Pekar, *Untersuchungen uber die Elektronentheorie der Kristalle* (Akademische-Verlag, Berlin, 1954).
[3] H. Fröhlich, Advances in Phys. 3, 325 (1954).
[4] G. Hohler, Z. Physik 140, 192 (1955).
[5] R. P. Feynman, Phys. Rev. 97, 660 (1955). These papers contain references to earlier work.